Sensors and Actuators B 153 (2011) 373–381

Contents lists available at ScienceDirect

Sensors and Actuators B: Chemical

journal homepage: www.elsevier.com/locate/snb

Effects of morphologies on acetone-sensing properties of tungsten trioxide nanocrystals

Deliang Chen[a,b,*], Xianxiang Hou[a], Tao Li[a], Li Yin[a], Bingbing Fan[a], Hailong Wang[a], Xinjian Li[b], Hongliang Xu[a], Hongxia Lu[a], Rui Zhang[a,c], Jing Sun[d]

[a] School of Materials Science and Engineering, Zhengzhou University, 100 Science Road, Zhengzhou 450001, PR China
[b] School of Physics and Engineering, Zhengzhou University, 100 Science Road, Zhengzhou 450001, PR China
[c] Laboratory of Aeronautical Composites, Zhengzhou Institute of Aeronautical Industry Management, University Centre, Zhengdong New District, Zhengzhou 450046, PR China
[d] The State Key Laboratory of High Performance Ceramics and Superfine Microstructure, Shanghai Institute of Ceramics, Chinese Academy of Sciences, 1295 Dingxi Road, Shanghai 200050, PR China

ARTICLE INFO

Article history:
Received 18 August 2010
Received in revised form 29 October 2010
Accepted 1 November 2010
Available online 10 November 2010

Keywords:
Tungsten oxide
Chemical sensor
Acetone
Gas sensing
Nanoplate
Nanoparticle

ABSTRACT

In this work, triclinic WO_3 nanoplates and WO_3 nanoparticles were comparatively investigated as sensing materials to detect acetone vapors. Single-crystalline WO_3 nanoplates with large side-to-thickness ratios were synthesized via a topochemical conversion from tungstate-based inorganic–organic hybrid nanobelts, and the WO_3 nanoparticles were obtained by calcining commercial H_2WO_4 powders at 550 °C. The acetone-sensing properties were evaluated by measuring the change in electrical resistance of the WO_3 sensors before and after exposure to acetone vapors with various concentrations. The WO_3 nanoplate sensors showed a high and stable sensitive response to acetone vapors with a concentration range of 2–1000 ppm, and the sensitivity was up to 42 for 1000 ppm of acetone vapor operating at 300 °C. The response and recovery times were as short as 3–10 s and 12–13 s, respectively, for the WO_3 nanoplate sensors when operating at 300 °C. The acetone-sensing performance of the WO_3 nanoplate sensors was more excellent than that of the WO_3 nanoparticle sensors under a similar operating condition. The enhancement of the WO_3 nanoplate sensors in the acetone-sensing property was attributed to the poriferous textures, single-crystalline microstructures and high surface areas of the aggregates consisting of WO_3 nanoplates, which were more favorable in rapid and efficient diffusion of acetone vapors than the WO_3 nanoparticles.

1. Introduction

Chemical sensors on the basis of semiconductor metal oxide nanomaterials have extensively been developed to detect volatile organic reagents and toxic gases [1–16]. The general mechanism of the oxide semiconductor sensors is based on the changes in electrical properties before and after exposure to the target gases or vapors [1]. Acetone, a common reagent widely used in industries and labs, is harmful to health, and it is also a biomarker for diagnosis of diabetes [2]. Recently, there is increasing attention attracted on the investigation of acetone-sensing materials and devices [3–16]. ZnO-based nanocrystals [3–6], perovskite ABO_3-type oxides [7–9], SnO_2-based nanocrystals [10–15] and La_2O_3 nanocrystals [16] have been investigated as the sensitive materials for the detection of acetone vapor at various concentration levels.

Tungsten oxides, *n*-type semiconductor materials with a band gap of 2.5–3.0 eV, have widely been investigated as photocatalysts [17], electrochromic materials [18] and electrodes for solar cells [19]. Recently, tungsten oxide nanocrystals have also been found to be promising candidate materials for gas-sensing applications [20]. WO_3 nanowires [21–23], WO_3 nanofibers [24], WO_3 hollow microspheres [25], WO_3 nanocrystals [26,27], WO_3 thin films [28] and h-WO_3/MWCNTs composites [1] have been used as the sensing materials for the detection of nitrogen oxides (N_2O, NO, NO_2). The sensors based on $W_{18}O_{49}$ nanowires [29], h-WO_3 nanocrystals [30], (Cr, V, Cu)-added WO_3 powders [31] and Cr-doped WO_3 nanocrystals [32] have been reported for NH_3 sensing applications. WO_3-based nanocrystals and films have also been investigated for gas-sensing applications in H_2 [28,33], ethanol [34,35], CO [36], H_2S [37], ozone [38] and humidity [39]. As far as we know, there are few reports on the acetone-sensing property of WO_3 nanocrystals [20].

* Corresponding author at: School of Materials Science and Engineering, Zhengzhou University, 100 Science Road, Zhengzhou 450001, PR China.
Tel.: +86 371 63888408; fax: +86 371 63888408.
E-mail address: dlchen@zzu.edu.cn (D. Chen).

0925-4005/$ – see front matter © 2010 Elsevier B.V. All rights reserved.
doi:10.1016/j.snb.2010.11.001

Recently, we developed a facile and efficient route to synthesize ultrathin WO_3 nanoplates with large side-to-thickness ratios, using tungstate-based inorganic–organic hybrid nanobelts as the precursors [40,41]. Our further research indicated the sensors using the above WO_3 nanoplates as the sensing material showed a highly sensitive property to alcohols [42].

In this work, we investigate the acetone sensing properties of the two-dimensional WO_3 nanoplates derived from a topochemical conversion route. For purposes of investigating the morphological effects, we also synthesize WO_3 nanoparticles by calcining commercial H_2WO_4 powders, and their acetone-sensing properties are also investigated. The related mechanisms for gas sensing are discussed.

2. Materials and methods

WO_3 nanoplates were synthesized according to our previously reported methods with some modification [40]. Firstly, $H_2W_2O_7{\cdot}xH_2O$ powders were prepared by leaching $[Bi_2O_2]$ layers from layered $Bi_2W_2O_9$ using an HCl aqueous solution [43]. Secondly, the as-obtained $H_2W_2O_7{\cdot}xH_2O$ powders reacted with *n*-octylamine in a nonpolar solvent of heptane to form tungstate-based inorganic–organic hybrid nanobelts with a lamellar microstructure, alternately consisting of inorganic $[WO_6]$ layers and organic ammonium layers [41]. Thirdly, removal of the organic ammonium layers from the tungstate-based inorganic–organic hybrid nanobelts led to the formation of ultrathin plate-like H_2WO_4 nanosized particles. Finally, the as-obtained H_2WO_4 nanoplates were then calcined at 250 °C for 5 h in air to synthesize WO_3 nanoplates. For purposes of comparison, commercial H_2WO_4 powders (AR, Sinopharm Chemical Reagent Co., Ltd.) were calcined at 550 °C for 2 h to prepare WO_3 nanoparticles.

The phase compositions of the products were determined by X-ray diffraction (XRD, Rigaku D/Max-3B diffractometer with Cu Kα radiation). The morphologies of the as-obtained products were observed on a scanning electron microscope (SEM, JEOL JSM-5600, 10 kV, coating Au) and a transmission electron microscope (TEM, JEOL JEM-2100F, 200 kV). The cell parameters of the products were calculated on the basis of their XRD patterns using a UnitCell program (by TJB Holland and SAT Redfern, 1995) by minimizing the sum of squares of residuals in 2θ.

The as-obtained WO_3 nanoplates (or nanoparticles) were used to make sensors for investigation of their acetone-sensing performance using a similar method reported in Ref. [42]. WO_3 nanoplates (or nanoparticles) were firstly mixed with a small amount of de-ionized H_2O to form WO_3 pastes in a glass dish. The WO_3 pastes were then coated onto the surfaces of an Al_2O_3 microtube with four Pt electrodes. After the WO_3 coating was air-dried, the coating process was repeated until a complete coating was formed. The WO_3-coated Al_2O_3 microtube was then fixed to a special pedestal with 6 poles by welding the four Pt electrodes to 4 poles of the pedestal, respectively. A heating coil was then inserted through the Al_2O_3 microtube and its two ends were welded to the other two poles of the pedestal.

The acetone sensing response of the WO_3 nanoplate or nanoparticle sensors was measured using a commercial computer-controlled HW-30A system under a static testing condition. The sensors, integrated in a large circuit board with 32 inlet-sites, were encased in a transparent glass chamber with a volume of 13.8 L. The testing system was placed in a ventilating cabinet with a large draught capacity. Acetone vapors with various concentrations were used as the target gases to characterize the sensing performance of the WO_3 sensors. Acetone was sampled using a syringe-like sampler. Liquid acetone was injected to a hot stage located in the chamber, and then the liquid acetone evaporated quickly to form an acetone vapor. The acetone vapor concentrations (2–1000 ppm) were calculated according to the acetone density and the volume of the chamber. The amounts ($V_{acetone}$, μL) of liquid acetone were determined according to Eq. (1).

$$V_{acetone} = \frac{10^{-9} V_0 \cdot M \cdot C_{acetone}}{22.4\rho \cdot p} \quad (1)$$

Here, V_0 is the volume of the chamber (V_0 = 13.8 L), ρ is the density of acetone (g cm^{-3}), M is the mole mass (g mol^{-1}) of acetone, p is the rate of purity of acetone, and $C_{acetone}$ is the acetone concentration (ppm). The operating temperature was 100–300 °C, controlled by an electric heating system. The relative humidity (RH) was 30–40%.

The WO_3 sensor (R) is connected in series with a load resistor (R_0) with a known resistance (22–1700 KΩ), and a source voltage (U_0) of 5 V is loaded on the circuit [42]. The system measured the voltages (U) loaded on the resistor R_0, and the resistances (R) of the WO_3 sensors can therefore be calculated according to Eq. (2). For the reducing gas of acetone and *n*-type semiconducting WO_3 sensors, the sensitivity (S_r) is defined as Eq. (3), where R_a and R_g are the resistances of the WO_3 sensor in air ambient and in acetone ambient, respectively. The response time (T_{res}) is defined as the time required for the sensor to reach 90% of the stabilized value of its resistance in the presence of the test gas. Similarly, the recovery time (T_{rec}) is defined as the time required for the sensor to reach 10% of the initial steady state value of its resistance after the gas was removed.

$$R = \frac{U_0 - U}{U} \times R_0 \quad (2)$$

$$S_r = \frac{R_a}{R_g} \quad (3)$$

3. Results and discussion

Fig. 1a shows the XRD pattern of the WO_3 nanoplates derived from tungstate-based inorganic–organic hybrid nanobelts. As Fig. 1a shows, there are intense peaks at 2θ = 23.19°, 23.72° and 24.44°, and these diffraction peaks can readily be indexed to 0 0 2, 0 2 0 and 2 0 0 reflections of a triclinic WO_3 phase (S.G.: P1 [1]), respectively, according to the literature data (JCPDS card No. 32-1395). According to its XRD result, the cell parameters of the WO_3 nanoplates are calculated to be a = 0.728(2) nm, b = 0.751(2) nm,

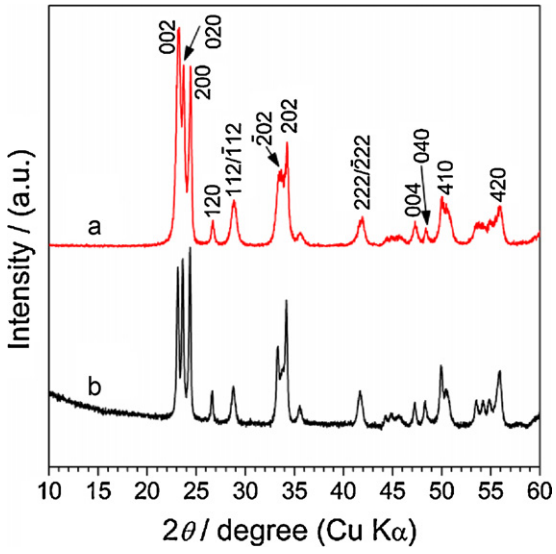

Fig. 1. Typical XRD patterns of (a) the WO_3 nanoplates derived from tungstate-based inorganic–organic hybrid nanobelts and (b) the WO_3 nanoparticles from commercial H_2WO_4 powders.

$c = 0.769(2)$ nm, $\alpha = 88.6(2)^\circ$, $\beta = 91.1(3)^\circ$ and $\gamma = 91.0(3)^\circ$, which are close to the literature values ($a = 0.7309$ nm, $b = 0.7522$ nm, $c = 0.7678$ nm, $\alpha = 88.81^\circ$, $\beta = 90.92^\circ$, $\gamma = 90.93^\circ$). In the previous report, we indexed the WO_3 nanoplates to a monoclinic phase [40], but our further refined results indicate that the calculated cell parameters of the WO_3 nanoplates are closer to a triclinic phase than a monoclinic one. Fig. 1b shows the XRD pattern of the WO_3 nanoparticles derived from commercial H_2WO_4 powders. There are intense reflections at $2\theta = 23.13^\circ$, 23.60° and 24.37°, which can also be indexed to a triclinic WO_3 phase. The calculated cell parameters are $a = 0.731(1)$ nm, $b = 0.754(1)$ nm, $c = 0.770(1)$ nm, $\alpha = 88.2(1)^\circ$, $\beta = 91.4(1)^\circ$, $\gamma = 90.5(1)^\circ$, which are close to those of WO_3 nanoplates. The (0 0 2) reflection in Fig. 1b is the third largest peak in relative intensity, similar to the literature data. When comparing Fig. 1a and b, one can easily find that the (0 0 2) reflection in Fig. 1a is the first largest peak. The enhanced intensity indicates that the WO_3 nanoplates present a preferred orientation along the [0 0 2] direction. Also, one can find that the peaks in Fig. 1b are sharper than the corresponding ones in Fig. 1a, indicating that the WO_3 nanoplates have a smaller crystal size than that of the WO_3 nanoparticles. In fact, the WO_3 nanoplates have a specific surface area of 180 m^2/g, according to the BET result [40].

Fig. 2a–d shows the typical TEM observations of WO_3 nanoplates derived from the tungstate-based inorganic–organic hybrid nanobelts. The low-magnification TEM image (Fig. 2a) indicates that the product obtained is of a predominant plate-like morphology according to the shallow contrast. Fig. 2b shows a single nanoplate with a dimension of *ca.* 200 nm × 400 nm. A typical HRTEM image of a WO_3 nanoplate is shown in Fig. 2c. The clear two-dimensional ordered lattice structure indicates that the obtained WO_3 nanoplate is single-crystalline. The interplanar distance values of *ca.* 0.364 and 0.376 nm can be readily assigned to the reflections from (2 0 0) and (0 2 0) planes of triclinic WO_3, respectively. Its corresponding SAED pattern is shown in Fig. 2d. The uniform, wide and ordered diffraction spots can be assigned to a single-crystalline triclinic WO_3 phase along the [0 0 2] zone axis. The TEM observation of the WO_3 nanoplates is very close to our previous report [40]. Since the WO_3 nanoplate is lying along the

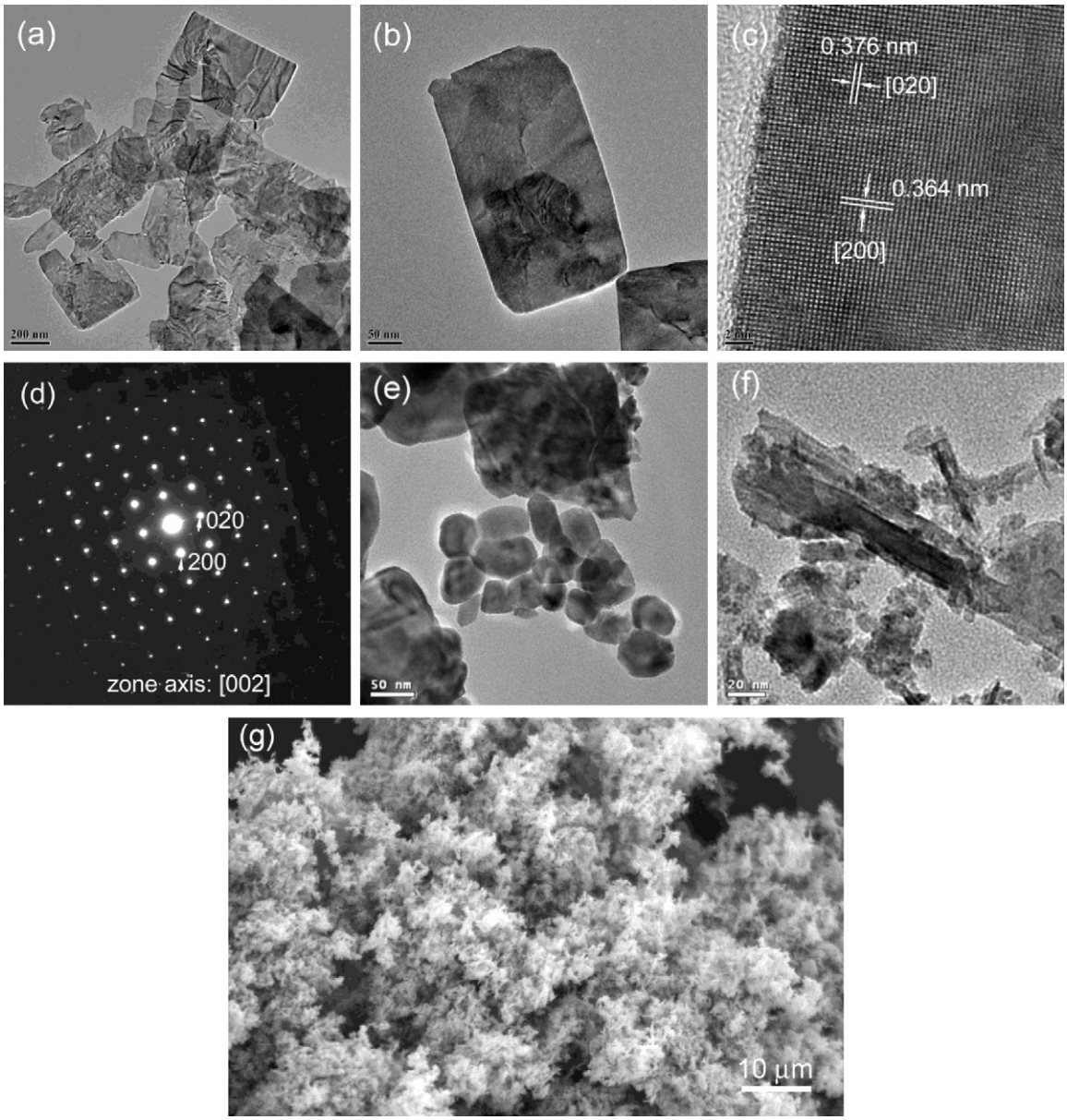

Fig. 2. (a and b) TEM images, (c) HRTEM image and (d) SAED pattern of WO_3 nanoplates; TEM images of (e) WO_3 nanoparticles and (f) the corresponding commercial H_2WO_4 powders; (g) SEM image of the as-obtained WO_3 nanoplates.

Cu grid, the thickness of the WO_3 nanoplate can be considered to be the [0 0 2] direction (*i.e.*, *c*-axis). The point is also corroborated by the XRD result that the WO_3 nanoplates show a higher intensity from the (0 0 2) plane than that of the WO_3 nanoparticles, as shown in Fig. 1.

Fig. 2e shows a typical TEM image of the WO_3 nanoparticles obtained from commercial H_2WO_4 powders. There are several morphologies, including spherical nanoparticles with sizes of 30–60 nm and plate-like aggregates with sizes 200–300 nm. The morphology of their precursor of H_2WO_4 is shown in Fig. 2f. It consists of particles with various sizes and shapes, including small nanoparticles with sizes of several nanometers, one-dimensional nanostructures with apparent diameters of 10–40 nm and lengths of 100–150 nm, and large particle aggregates with sizes of about 100 nm. Due to the wide size-distribution and multi-shapes of the H_2WO_4 powders, the resultant WO_3 nanoparticles accordingly take on diversiform morphologies with various sizes.

Fig. 3 shows the acetone-sensing response profiles of the sensors made using the as-obtained WO_3 nanoplates as the sensitive material. Fig. 3a shows a typical response profile of the WO_3 nanoplate sensors operating at 300 °C to acetone vapors with various concentrations from 2 ppm to 1000 ppm. One can find that there are sharp rises and drops in *U* values when the acetone vapors are injected and discharged, respectively, which indicates that the WO_3 nanoplate sensors are of fast response and recovery speeds to acetone vapors. Fig. 3b shows a similar rapid acetone-sensitive response of the WO_3 nanoplate sensors at an operating temperature of 250 °C. When we compare the *U* values of Fig. 3a and b, the change amounts in *U* of the WO_3 nanoplate sensors operating at 250 °C are less than those of the WO_3 nanoplate sensors operating at 300 °C. Fig. 3c shows typical response results of the WO_3 nanoplate sensors operating at 200 °C, and Fig. 3d shows the response curve operating at 100 °C. One can find that when the operating temperature decreases to 100 °C, the change amounts in *U* obviously decrease, the response speed and the detectable limits decrease, and the response profiles become instable, as shown in Fig. 3a–d.

Fig. 4a presents the sensitivities (R_a/R_g) of the WO_3 nanoplate sensors operating at various temperatures and acetone concentrations. As Fig. 4a shows, the sensitivities of the WO_3 nanoplate sensors decrease as the operating temperature decreases in the range of 100–300 °C under the same acetone concentrations in the range of 2–1000 ppm. Also, we can find that the sensitivity

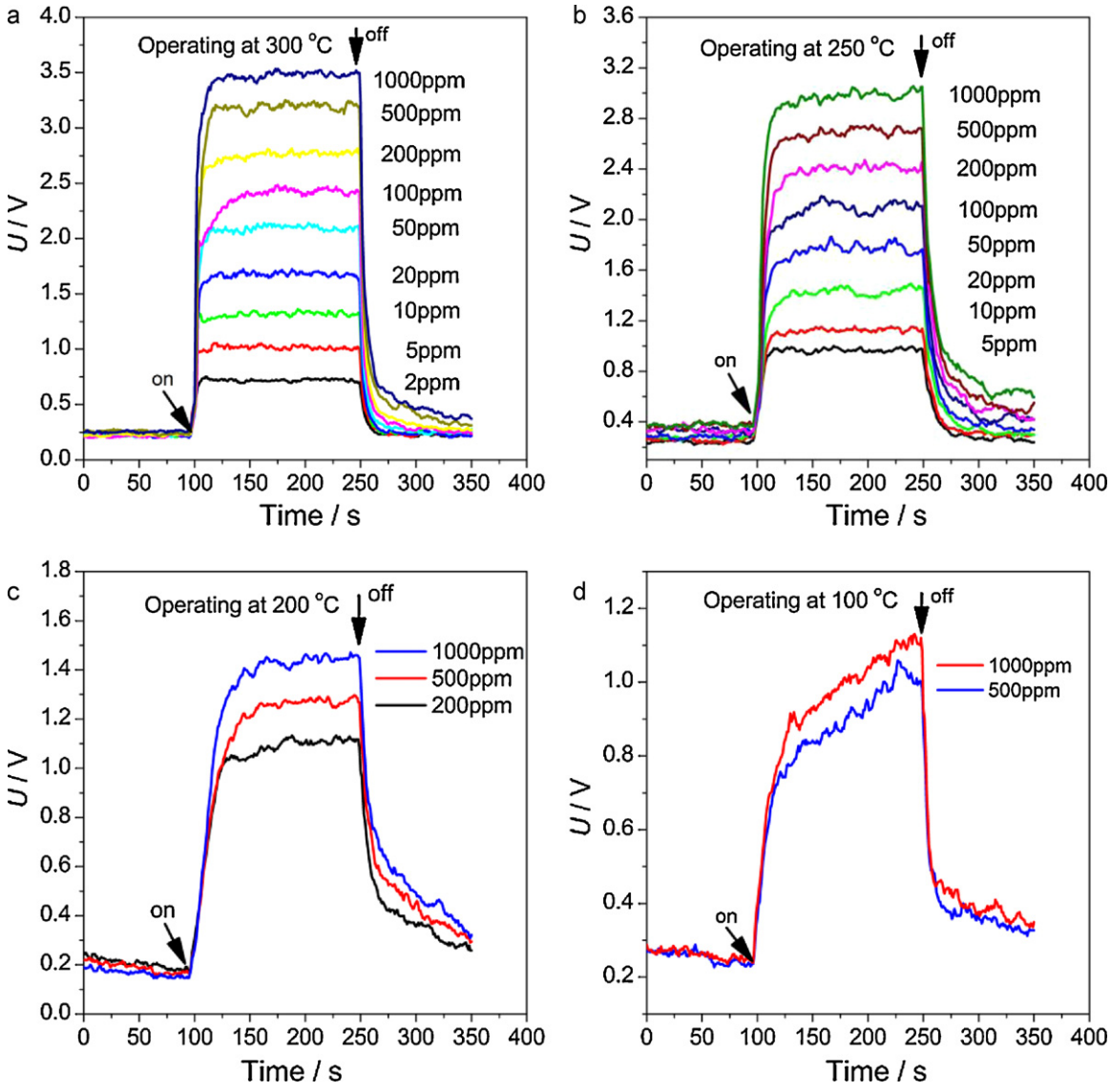

Fig. 3. Acetone-sensing response profiles of the WO_3 nanoplate sensors operating at various temperatures and various acetone vapor concentrations. The R_0 values are 22 kΩ, 100 kΩ, 100 kΩ and 470 kΩ, respectively, for the measurements operating at (a) 300 °C, (b) 250 °C, (c) 200 °C and (d) 100 °C.

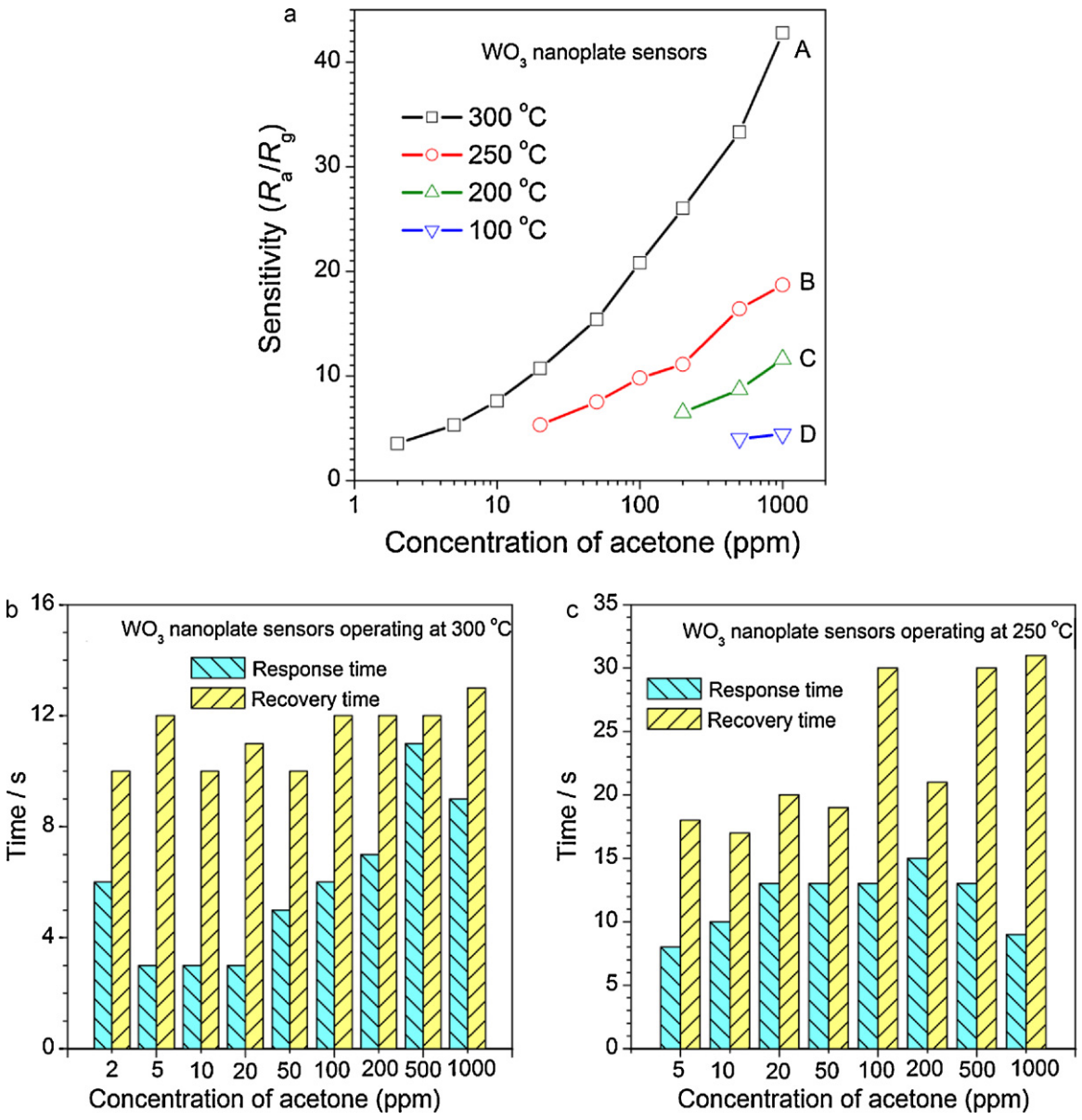

Fig. 4. (a) Sensitivities of the WO_3 nanoplate sensors as a function of the concentration of acetone vapor at various operating temperatures, and (b and c) response and recovery times of the WO_3 nanoplate sensors to acetone vapor with various concentrations operating at (b) 300 °C and (c) 250 °C.

increases with an increase in the acetone concentration at the same operating temperature, which is similar to the results of the $La_{0.68}Pb_{0.32}FeO_3$ sensors [7]. At an operating temperature of 300 °C, the WO_3 nanoplate sensor has a sensitivity as high as 42 for a 1000 ppm acetone vapor, and it has a detectable limit as low as 2 ppm of acetone vapor with a sensitivity of about 4, as shown as curve A. At a low operating temperature of 100 °C, the sensitivities of the WO_3 nanoplate sensors are about 3 for 100–500 ppm acetone vapors (curve D in Fig. 4a).

Fig. 4b and c shows the response and recovery times of the WO_3 nanoplate sensors under various concentrations of acetone vapors at operating temperatures of 250–300 °C. As Fig. 4b shows, the response times of the WO_3 nanoplate sensors operating at 300 °C are 3–10 s in the vapor concentration range of 2–1000 ppm, and their corresponding recovery times are 6–13 s. For the case of the response of the WO_3 nanoplate sensors operating at 250 °C, as shown in Fig. 4c, the response times lie in a range of 8–15 s, and their recovery times are 15–31 s. Both the response times and recovery times increase with the increase in operating temperature.

For purposes of comparison, Fig. 5 shows the acetone-sensing response profiles of the WO_3 nanoparticle sensors using the calcined products of commercial H_2WO_4 powders as the sensing material. Fig. 5a–c presents the typical results operating at 300 °C, 250 °C and 200 °C, respectively. At relative high operating temperatures of 250–300 °C (Fig. 5a and b), the WO_3 nanoparticle sensors show a rapid and detectable response to acetone vapors with concentrations of 2–1000 ppm, whereas the response profiles become not typical at an operating temperature of 200 °C, as shown in Fig. 5c.

The sensitivities of the WO_3 nanoparticle sensors are shown in Fig. 6a. The sensitivity of the WO_3 nanoparticle sensor increases with the increase of acetone concentration from 2 for 2 ppm of acetone vapor to 19 for 1000 ppm of acetone vapor, operating at 300 °C, as shown as curve A in Fig. 6a. For the cases of operating at 250 °C and 200 °C, as shown as curves B and C in Fig. 6a, their sensitivi-

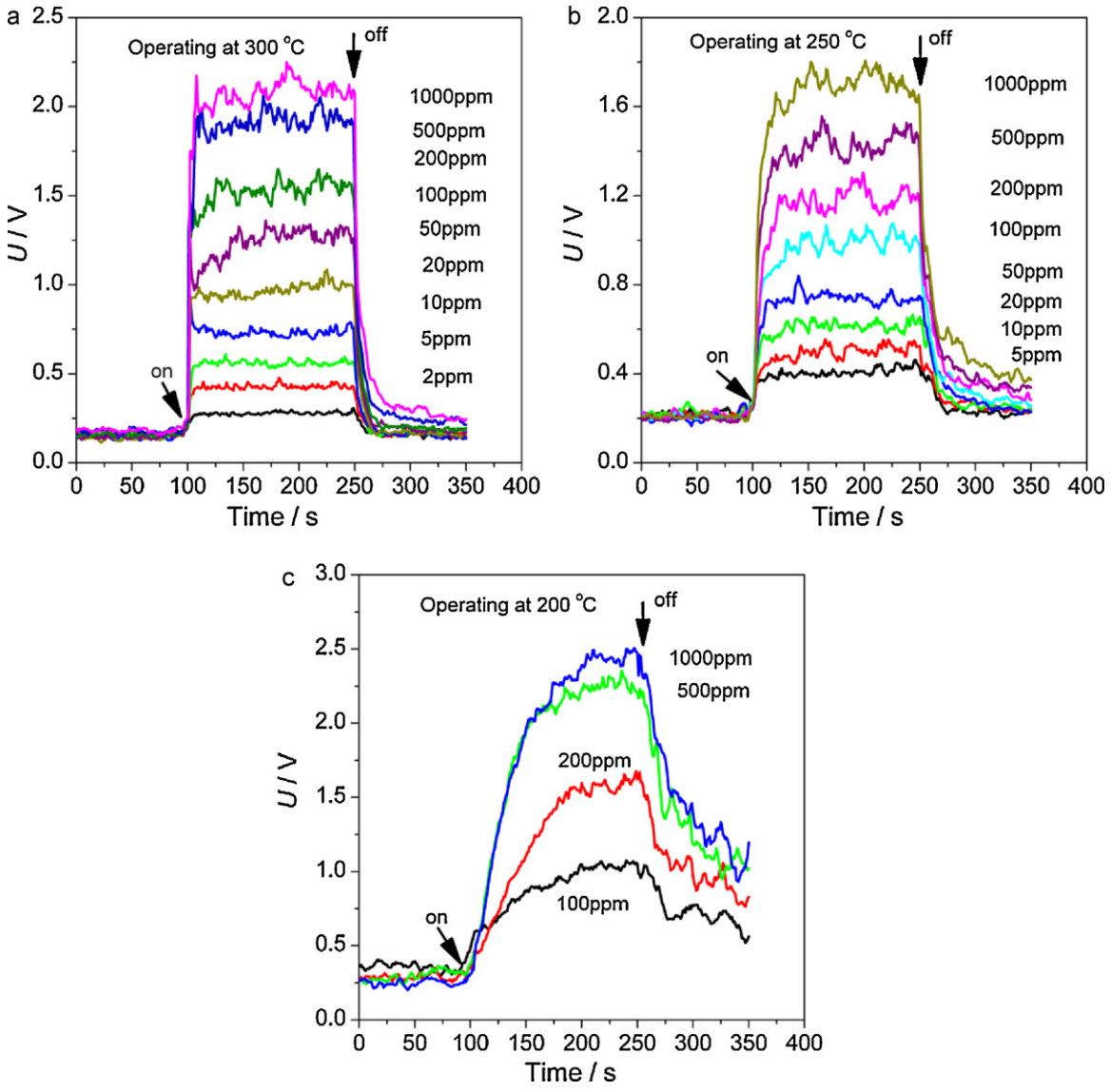

Fig. 5. Acetone-sensing response profiles of the WO_3 nanoparticle sensors operating at various temperatures and various acetone vapor concentrations. The R_0 values are 47 kΩ, 470 kΩ and 1700 kΩ, respectively, for the measurements operating at (a) 300 °C, (b) 250 °C and (c) 200 °C.

ties increase with the increase in concentrations of acetone vapors, but the values are less than 15. The change trends in sensitivity of the WO_3 nanoparticle sensors are similar to those of the WO_3 nanoplate sensors (Fig. 4a).

Fig. 6b shows the response times of the WO_3 nanoparticle sensors operating at 300 °C under acetone vapors with various concentrations of 2–1000 ppm. The response times are less than 10 s in the testing concentration range, and the corresponding recovery times are 10–17 s. When the operating temperature decreases to 250 °C, the response times are 4–20 s, and their recovery times are 17–35 s, as shown in Fig. 6c.

When comparing the acetone-response properties (Figs. 3 and 4) of the WO_3 nanoplate sensors and those (Figs. 5 and 6) of the WO_3 nanoparticle sensors, we can reach the following points: (1) the WO_3 nanoplate sensors have much higher sensitivities than the WO_3 nanoparticle sensors in an acetone concentration range of 2–1000 ppm at operating temperatures of 250–300 °C; (2) the WO_3 nanoplate sensors have faster response speeds than the WO_3 nanoparticle sensors; (3) the WO_3 nanoplate sensors show more stable response performance than the WO_3 nanoparticle sensors.

The enhancement in acetone-response properties of the WO_3 nanoplate sensors should be attributed to the ultrathin two-dimensional plate-like morphology of the single-crystalline WO_3 nanoplates, derived from tungstate-based inorganic–organic hybrid nanobelts via a topochemical conversation route. The ultrathin WO_3 nanoplates with large side-to-thickness ratios show a favorable tendency to form loose and poriferous aggregates in a natural manner. In fact, this poriferous microstructure can be clearly corroborated by the SEM observation, as shown in Fig. 2g. The loose and poriferous structured aggregates provide numerous channels for the efficient and rapid diffusion of acetone vapors [42]. Also, the plate-like morphology of the WO_3 nanoplates is helpful to form an interconnected film for the gas-sensing applications. Furthermore, the single-crystalline structure of the WO_3 nanoplates provides a favorable precondition both for the rapid sorption–desorption of acetone vapors and for the high efficient circulation of electrons produced in the response process, because of the large surface areas and the low rates of crystalline defections for the WO_3 nanoplates. Whereas for the WO_3 nanoparticles from commercial H_2WO_4 powders, their morphologies are not uniform and their sizes are large,

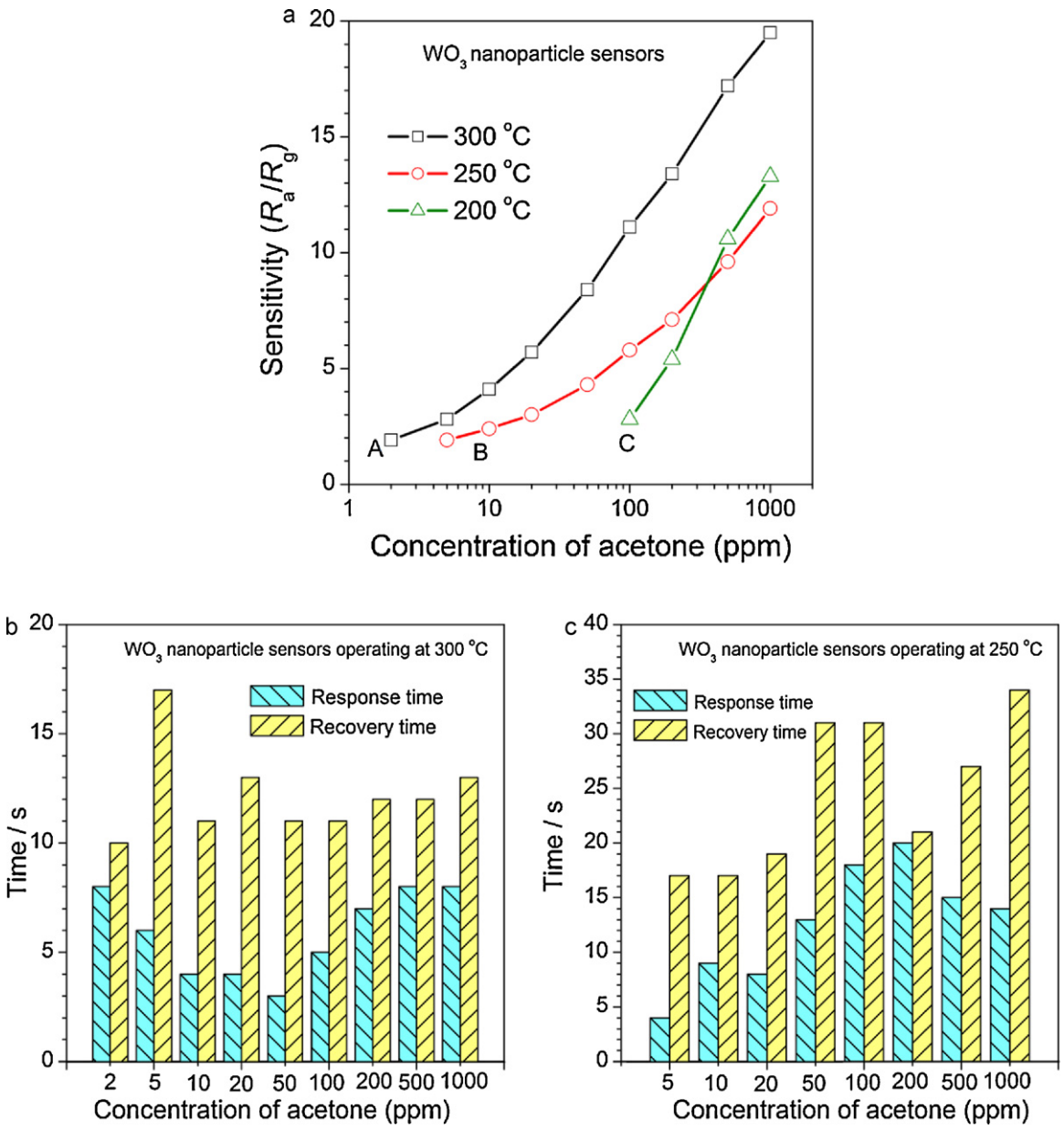

Fig. 6. (a) Sensitivities of the WO_3 nanoparticle sensors as a function of the concentration of acetone vapor at various operating temperatures, and (b and c) response and recovery times of the WO_3 nanoparticle sensors to acetone vapor with various concentrations operating at (b) 300 °C and (c) 250 °C.

which led to hard aggregates (Fig. 2e). Therefore, the morphological difference between the WO_3 nanoplates from hybrid precursors and the WO_3 nanoparticles from commercial H_2WO_4 powders and the difference in textures of the resultant aggregates account for the different performance of the WO_3 sensors toward acetone vapors with various concentrations operating at 100–300 °C.

The gas-sensing mechanisms for the same type semiconductors are usually of some similarity, and WO_3 is an *n*-type semiconductor, similar to ZnO and SnO_2 [42]. Therefore, the acetone-sensing mechanisms of WO_3 nanocrystals are also similar to those of ZnO and SnO_2 nanocrystals [5,13], and can be explained using a depletion-layer model [44]. For acetone vapor sensing of WO_3 nanocrystals, oxygen sorption plays a critical role in the electrical resistance. In an air environment, the oxygen ionosorption depletes conduction electrons and then enhances the resistance of the WO_3 sensors, whereas their resistance can sharply decrease upon exposure to the reducing substance of acetone vapor.

When the WO_3 sensors are exposed to air, the O_2 molecules in air react with WO_3 and produce oxygen species of O_2^-, O^{2-} and O^-, which are adsorbed on the surfaces of WO_3 nanocrystals at an elevated temperature. The amounts of the oxygen species adsorbed are strongly dependent on the operating temperature, and the higher the operating temperature, the larger the amounts of O^{2-} and O^- are in the testing temperature range [5]. The related reaction kinetics can be described as Eqs. (4)–(6).

$$O_2(\text{gas}) \leftrightarrow O_2(\text{adsorbed}) \quad (4)$$

$$O_2(\text{adsorbed}) + e^- \leftrightarrow O_2^- \quad (5)$$

$$O_2^- + e^- \leftrightarrow 2O^- \quad (6)$$

When the WO_3 sensors are exposed to acetone vapors, the ionic oxygen species adsorbed on the surface of WO_3 nanocrystals react with reducing acetone molecules, as shown as Eqs. (7)–(9) [5]. The released electrons in the reactions compensate to the conduction

band, and thus enhance the conductance of the WO_3 sensors [13].

$$CH_3COCH_3 + O^- \rightarrow CH_3C^+O + CH_3O^- + e^- \quad (7)$$

$$CH_3C^+O \rightarrow C^+H_3 + CO \quad (8)$$

$$CO + O^- \rightarrow CO_2 + e^- \quad (9)$$

According to the above acetone-sensing mechanism, one can easily conclude that large surface areas, high crystallinity, and expedite diffusion channels of WO_3 nanocrystals are favorable in enhancing the acetone-sensing performance of the resultant sensors. The WO_3 nanoplates with high specific surface areas ($\sim$180 m^2/g^{-1}) and high crystallinity are of more excellent acetone-sensing properties than the WO_3 nanoparticles in this work.

Cao and co-workers [20] reported an acetone-sensing result of WO_3 nanotubes and found that the WO_3 nanotube sensors had a peak sensitivity of 32.7 at 340 °C for a 5×10^{-5} mol/L acetone vapor, but the sensitivities were less than 20 when the operating temperatures were lower and higher than 340 °C. More and co-workers [11] reported the acetone-sensing property of Co-doped SnO_2 thin films, but their response and recovery times were longer than 100 s even at an operating temperature higher than 300 °C. Xu and co-workers [13] investigated the acetone-sensing performance of SnO_2 nanowire sensors, but their peak sensitivity was less than 10. Therefore, the WO_3 nanoplate sensors reported here are of good overall properties to acetone sensing applications comparing these literature results.

4. Conclusions

We have comparatively investigated the acetone-sensing properties of the WO_3 nanoplates from tungstate-based inorganic–organic hybrid nanobelts and the WO_3 nanoparticles from commercial H_2WO_4 powders in an acetone-concentration range of 2–1000 ppm operating at 100–300 °C. The WO_3 nanoplate sensors showed a high and stable sensitive response to acetone vapors, and the sensitivity was up to 42 for 1000 ppm of acetone vapor operating at 300 °C. The response and recovery times were as short as 3–10 s and 12–13 s, respectively, for the WO_3 nanoplate sensors when operating at 300 °C. The acetone-sensing performance of the WO_3 nanoplate sensors was more excellent than that of the WO_3 nanoparticle sensors under a similar operating condition. The enhancement of the WO_3 nanoplate sensors in the acetone-sensing property could be attributed to the poriferous textures, single-crystalline microstructures and high surface areas of the aggregates consisting of WO_3 nanoplates, which were favorable in rapid and efficient diffusion of acetone vapors.

Acknowledgements

This work was supported by the National Natural Science Foundation of China (No. 50802090), the China Postdoctoral Science Foundation (No. 20090450094), the Opening Project of State Key Laboratory of High Performance Ceramics and Superfine Microstructure (No. SKL200905SIC) and the Introduced Talent Project of Zhengzhou University. D. Chen thanks Professor Yoshiyuki Sugahara (Waseda University) for his valuable discussion on the formation mechanism of the tungstate-based inorganic–organic hybrid nanobelts.

References

[1] C. Balási, K. Sedláková, E. Llobet, R. Ionescu, Novel hexagonal WO_3 nanopowder with metal decorated carbon nanotubes as NO_2 gas sensor, Sens. Actuators B: Chem. 133 (2008) 151–155.
[2] L. Wang, X. Yun, M. Stanacevic, P.I. Gouma, An acetone nanosensor for non-invasive diabetes detection, Olfaction Electron. Nose 1137 (2009) 206–208.
[3] Y. Anno, T. Maekawa, J. Tamaki, Y. Asano, K. Hayashi, N. Miura, N. Yamazoe, Zinc-oxide-based semiconductor sensors for detecting acetone and capronaldehyde in the vapour of consommé soup, Sens. Actuators B: Chem. 25 (1995) 623–627.
[4] P.P. Sahay, Zinc oxide thin film gas sensor for detection of acetone, J. Mater. Sci. 40 (2005) 4383–4385.
[5] S.J. Chang, T.J. Hsueh, I.C. Chen, S.F. Hsieh, S.P. Chang, C.L. Hsu, Y.R. Lin, B.R. Huang, Highly sensitive ZnO nanowire acetone vapor sensor with Au adsorption, IEEE T. Nanotechnol. 7 (2008) 754–759.
[6] Y. Zeng, T. Zhang, M.X. Yuan, M.H. Kang, G.Y. Lu, R. Wang, H.T. Fan, Y. He, H.B. Yang, Growth and selective acetone detection based on ZnO nanorod arrays, Sens. Actuators B: Chem. 143 (2009) 93–98.
[7] L. Zhang, H. Qin, P. Song, J. Hu, M. Jiang, Electric properties and acetone-sensing characteristics of $La_{1-x}Pb_xFeO_3$ perovskite system, Mater. Chem. Phys. 98 (2006) 358–362.
[8] X. Liu, J. Hu, B. Cheng, H. Qin, M. Jiang, Acetone gas sensing properties of $SmFe_{1-x}Mg_xO_3$ perovskite oxides, Sens. Actuators B: Chem. 134 (2008) 483–487.
[9] M. Yang, L.H. Huo, H. Zhao, S. Gao, Z.M. Rong, Electrical properties and acetone-sensing characteristics of $LaNi_{1-x}Ti_xO_3$ perovskite system prepared by amorphous citrate decomposition, Sens. Actuators B: Chem. 143 (2009) 111–118.
[10] J. Zhao, L.H. Huo, S. Gao, H. Zhao, J.G. Zhao, Alcohols and acetone sensing properties of SnO_2 thin films deposited by dip-coating, Sens. Actuators B: Chem. 115 (2006) 460–464.
[11] S.B. Patil, P.P. Patil, M.A. More, Acetone vapour sensing characteristics of cobalt-doped SnO_2 thin films, Sens. Actuators B: Chem. 125 (2007) 126–130.
[12] M.M. Zhang, G.S. Jiang, Gas sensing properties of Co_3O_4-loaded SnO_2 to ethanol and acetone, Chin. J. Chem. Phys. 20 (2007) 315–318.
[13] L. Qin, J. Xu, X. Dong, Q. Pan, Z. Cheng, Q. Xiang, F. Li, Template-free synthesis of square-shaped SnO_2 nanowires: the temperature effect and acetone gas sensors, Nanotechnology 19 (2008) 185705.
[14] C.H. Fang, S.Z. Wang, Q. Wang, J. Liu, B.Y. Geng, Coralloid SnO_2 with hierarchical structure and their application as recoverable gas sensors for the detection of benzaldehyde/acetone, Mater. Chem. Phys. 122 (2010) 30–34.
[15] A.A. Zvyagin, A.V. Shaposhnik, S.V. Ryabtsev, D.A. Shaposhnik, A.A. Vasil'ev, I.N. Nazarenko, Determination of acetone and ethanol vapors using semiconductor sensors, J. Anal. Chem. 65 (2010) 94–98.
[16] L. Tang, Y. Li, K. Xu, X. Hou, Y. Lv, Sensitive and selective acetone sensor based on its cataluminescence from nano-La_2O_3 surface, Sens. Actuators B: Chem. 132 (2008) 243–249.
[17] M. Sadakane, K. Sasaki, H. Kunioku, B. Ohtani, R. Abe, W. Ueda, Preparation of 3-D ordered macroporous tungsten oxides and nano-crystalline particulate tungsten oxides using a colloidal crystal template method, and their structural characterization and application as photocatalysts under visible light irradiation, J. Mater. Chem. 20 (2010) 1811–1818.
[18] N.A. Galiote, R.L.T. Parreira, J.M. Rosolen, F. Huguenin, Self-assembled films from WO_3: electrochromism and lithium ion diffusion, Electrochem. Commun. 12 (2010) 733–736.
[19] L. Meda, G. Tozzola, A. Tacca, G. Marra, S. Caramori, V. Cristino, C.A. Bignozzi, Photo-electrochemical properties of nanostructured WO_3 prepared with different organic dispersing agents, Solar Energy Mater. Solar Cells 94 (2010) 788–796.
[20] M. Kang, C. Cao, X. Xu, B. Lian, Molten-salt synthesis of tungsten oxide nanotubes: morphological and gas sensitivity, Chin. Sci. Bull. 53 (2008) 335–338.
[21] C.S. Rout, K. Ganesh, A. Govindaraj, C.N.R. Rao, Sensors for the nitrogen oxides, NO_2, NO and N_2O, based on In_2O_3 and WO_3 nanowires, Appl. Phys. A: Mater. Sci. Process. 85 (2006) 241–246.
[22] J. Polleux, A. Gurlo, N. Barsan, U. Weimar, M. Antonietti, M. Niederberger, Template-free synthesis and assembly of single-crystalline tungsten oxide nanowires and their gas-sensing properties, Angew. Chem. Int. Ed. 45 (2006) 261–265.
[23] B. Deb, S. Desai, G.U. Sumanasekera, M.K. Sunkara, Gas sensing behaviour of mat-like networked tungsten oxide nanowire thin films, Nanotechnology 18 (2007) 285501.
[24] S. Piperno, M. Passacantando, S. Santucci, L. Lozzi, S.L. Rosa, WO_3 nanofibers for gas sensing applications, J. Appl. Phys. 101 (2007) 124504.
[25] C.-Y. Lee, S.-J. Kim, I.-S. Hwang, J.-H. Lee, Glucose-mediated hydrothermal synthesis and gas sensing characteristics of WO_3 hollow microspheres, Sens. Actuators B: Chem. 142 (2009) 236–242.
[26] I. Jiménez, J. Arbiol, A. Cornet, J.R. Morante, Structural and gas-sensing properties of WO_3 nanocrystalline powders obtained by a sol–gel method from tungstic acid, IEEE Sens. J. 2 (2002) 329–334.
[27] S.-H. Wang, T.-C. Chou, C.-C. Liu, Nano-crystalline tungsten oxide NO_2 sensor, Sens. Actuators B: Chem. 94 (2003) 343–351.
[28] Y. Shen, T. Yamazaki, Z. Liu, D. Meng, T. Kikuta, N. Nakatani, Influence of effective surface area on gas sensing properties of WO_3 sputtered thin films, Thin Solid Films 517 (2009) 2069–2072.
[29] Y.M. Zhao, Y.Q. Zhu, Room temperature ammonia sensing properties of $W_{18}O_{49}$ nanowires, Sens. Actuators B: Chem. 137 (2009) 27–31.
[30] C. Balási, L. Wang, E.O. Zayim, I.M. Szilágyi, K. Sedlacková, J. Pfeifer, A.L. Tóh, P.I. Gouma, Nanosize hexagonal tungsten oxide for gas sensing applications, J. Eur. Ceram. Soc. 28 (2008) 913–917.
[31] F. Morazzoni, R. Scotti, L. Origoni, M. D'Arienzo, I. Jiméz, A. Cornet, J.R. Morante, Mechanism of NH_3 interaction with transition metal-added nanosized WO_3 for gas sensing: in situ electron paramagnetic resonance study, Catal. Today 126 (2007) 169–176.

[32] I. Jiménez, M.A. Centeno, R. Scotti, F. Morazzoni, J. Arbiol, A. Cornet, J.R. Morante, NH_3 interaction with chromium-doped WO_3 nanocrystalline powders for gas sensing applications, J. Mater. Chem. 14 (2004) 2412–2420.
[33] R. Calavia, A. Mozalev, R. Vazquez, I. Gracia, C. Can, R. Ionescu, E. Llobet, Fabrication of WO_3 nanodot-based microsensors highly sensitive to hydrogen, Sens. Actuators B: Chem. 149 (2010) 352–361.
[34] J. Ederth, J.M. Smulko, L.B. Kish, P. Heszler, C.G. Granqvist, Comparison of classical and fluctuation-enhanced gas sensing with Pd_xWO_3 nanoparticle films, Sens. Actuators B: Chem. 113 (2006) 310–315.
[35] Y.S. Kim, Thermal treatment effects on the material and gas-sensing properties of room-temperature tungsten oxide nanorod sensors, Sens. Actuators B: Chem. 137 (2009) 297–304.
[36] R.-J. Wu, W.-C. Chang, K.-M. Tsai, J.-G. Wu, The Novel CO sensing material CoOOH–WO_3 with Au and SWCNT performance enhancement, Sens. Actuators B: Chem. 138 (2009) 35–41.
[37] R. Ionescu, A. Hoel, C.G. Granqvist, E. Llobet, P. Heszler, Low-level detection of ethanol and H_2S with temperature- modulated WO_3 nanoparticle gas sensors, Sens. Actuators B: Chem. 104 (2005) 132–139.
[38] W. Belkacem, A. Labidi, J. Guérin, N. Mliki, K. Aguir, Cobalt nanograins effect on the ozone detection by WO_3 sensors, Sens. Actuators B: Chem. 132 (2008) 196–201.
[39] C.L. Dai, M.C. Liu, F.S. Chen, C.C. Wu, M.W. Chang, A nanowire WO_3 humidity sensor integrated with micro-heater and inverting amplifier circuit on chip manufactured using CMOS-MEMS technique, Sens. Actuators B: Chem. 123 (2007) 896–901.
[40] D. Chen, L. Gao, A. Yasumori, K. Kuroda, Y. Sugahara, Size- and shape-controlled conversion of tungstate-based inorganic–organic hybrid belts to WO_3 nanoplates with high specific surface areas, Small 4 (2008) 1813–1822.
[41] D. Chen, Y. Sugahara, Tungstate-based inorganic–organic hybrid nanobelts/nanotubes with lamellar mesostructures: synthesis, characterization, and formation mechanism, Chem. Mater. 19 (2007) 1808–1815.
[42] D. Chen, X. Hou, H. Wen, Y. Wang, H. Wang, X. Li, R. Zhang, H. Lu, H. Xu, S. Guan, J. Sun, L. Gao, The enhanced alcohol-sensing response of ultrathin WO_3 nanoplates, Nanotechnology 21 (2010) 035501.
[43] M. Kudo, H. Ohkawa, W. Sugimoto, N. Kumada, Z. Liu, O. Terasaki, Y. Sugahara, A layered tungstic acid $H_2W_2O_7{\cdot}nH_2O$ with a double-octahedral sheet structure: conversion process from an aurivillius phase $Bi_2W_2O_9$ and structural characterization, Inorg. Chem. 42 (2003) 4479–4484.
[44] L. Liao, H.B. Lu, J.C. Li, H. He, D.F. Wang, D.J. Fu, C. Liu, W.F. Zhang, Size dependence of gas sensitivity of ZnO nanorods, J. Phys. Chem. C 111 (2007) 1900–1903.

Biographies

Deliang Chen has been an associate professor at Zhengzhou University since 2007. He received his BS and MS degrees from Central South University in 1999 and 2002, respectively. Then he moved to Shanghai Institute of Ceramics, Chinese Academy of Sciences, where he received his PhD degree in Materials Science and Engineering in 2005. From April 2005 to March 2007, he moved to Waseda University to do postdoc research as Visiting Research Associate. His current research interests are focused on the fields of chemical sensors, photocatalysts, chemical synthesis of low-dimensional materials, intercalation chemistry, and super-hard materials.

Xianxiang Hou studied Applied Chemistry and received his BS degree from Zhengzhou Institute of Light Industry in 2008. He is currently a master course student at Zhengzhou University. His research includes the synthesis, characterization and sensing applications of low-dimensional metal oxide nanocrystals.

Tao Li studied Materials Science & Engineering and received his BS degree from Xi'an University of Technology in 2007. He is currently a master course student at Zhengzhou University. His research includes the synthesis, characterization and sensing applications of metal oxides/metal oxides complex nanocrystals.

Li Yin studied Materials Science & Engineering and received her BS degree from Zhengzhou University in 2002. She is currently a master course student at Zhengzhou University. Her research includes the synthesis, characterization and sensing applications of metal oxides/metals complex nanocrystals.

Bingbing Fan is now a lecturer at Zhengzhou University. She received her BS and PhD degrees from Zhengzhou University in 2006 and 2010, respectively. Her research interests are focused on the fields of computational materials and superhard materials.

Hailong Wang has been an associate professor at Zhengzhou University since 2007. He received his BS, MS and PhD degrees from Zhengzhou University in 2000, 2004 and 2007, respectively, in Materials Science and Engineering. His research interests are focused on the fields of superhard materials and superhigh temperature ceramics.

Xinjian Li is a professor at Zhengzhou University. He received his BS and MS degrees from Zhengzhou University, and received his PhD degree from China Science & Technology University. His current research interests are focused on photoelectrical properties and applications of semiconductor nanostructures.

Hongliang Xu has been an associate professor at Zhengzhou University since 2005. He received his BS degree from Henan Polytechnic University in 1991, MS degree from China University of Mining and Technology in 1999, and PhD degree from Tongji University in 2005. His current research interests are focused on the fields of superconductive materials, layered materials and ceramic composites.

Hongxia Lu has been a professor at Zhengzhou University since 2007. She received her BS and MS degrees from Huazhong University of Science and Technology in 1991 and 1994, respectively. Then she received her PhD degree from Zhengzhou University in 2005. Her current research interests are focused on electronic ceramic materials and nanomaterials.

Rui Zhang has been a professor at Zhengzhou University and Zhengzhou Institute of Aeronautical Industry Management. He received his BS and MS degrees from Tsinghua University in 1990 and 1995, and received his PhD degree from Shanghai Institute of Ceramics, Chinese Academy of Sciences in 2004. His current research interests include metal–ceramics, electronic ceramics and ceramic matrix composites.

Jing Sun has been a researcher at Shanghai Institute of Ceramics, CAS. She received her MS degree from Changchun Institute of Applied Chemistry, CAS in 1994, and received her PhD degree from Shanghai Institute of Ceramics, CAS in 1997. Her current research interests are focused on carbon nanotube composites and low-dimensional functional nanomaterials.